START-TO-END SIMULATIONS FOR AN X-RAY FEL OSCILLATOR AT THE LCLS-II AND LCLS-II-HE

W. Qin*, S. Huang, K. X. Liu, IHIP, Peking University, Beijing 100871, China
K.-J. Kim, R. R. Lindberg, ANL, Argonne, IL 60439, USA
Y. Ding, Z. Huang, T. Maxwell, K. Bane, G. Marcus, SLAC, Menlo Parck, CA 94025, USA

Abstract

The proposed high repetition-rate electron beam from the LCLS-II and LCLS-II High Energy (LCLS-II-HE) upgrade are promising sources as drivers for an X-ray FEL Oscillator (XFELO) operating at both the harmonic and fundamental frequencies. In this contribution we present start-to-end simulations for an XFELO operating at the fifth harmonic with 4 GeV LCLS-II beam and at the fundamental with 8 GeV LCLS-II-HE beam. The electron beam longitudinal phase space is optimized by shaping the photoinjector laser and adjusting various machine parameters. The XFELO simulations show that high-flux output radiation pulses with 10^{10} photons and 3 meV (FWHM) spectral bandwidth can be obtained with the 8 GeV configuration.

INTRODUCTION

X-ray free-electron lasers (XFELs) such as the LCLS [1] in self-amplified spontaneous emission (SASE) [2, 3] mode are now generating unprecedentedly bright X-ray pulses for wide range of applications. Reaching fully coherent, stable hard X-ray pulses is still challenging due to the stochastic nature of the SASE process. Hard X-ray self-seeding [4] improved the temporal coherence and brightness but still relies on a SASE seed. The transition to the era of high repetition rate XFELs provides promising opportunity for linac based X-ray FEL oscillator (XFELO) [5–8], which is characterized with full coherence, ultra narrow bandwidth and stable X-ray pulses. The XFELO relies on successive low gain amplification of X-ray pulses trapped in an optical cavity with crystal mirrors. Since the spectral acceptance of the crystal mirror is about ~10 meV, high quality electron beams with low emittance, low energy spread are required.

Feasibility study of 5th harmonic XFELO utilizing the LCLS-II [9] was carried out with an ideal 4 GeV beam for 14.4 keV photon energy [10, 11]. The proposed high energy upgrade of LCLS-II to 8 GeV LCLS-II-HE [12] enables driving the same wavelength in the fundamental mode. The performance of XFELO is strongly affected by the longitudinal phase space flatness due to the narrow spectral acceptance of the crystals. Linearizing longitudinal phase space via current shaping was studied [13]. Here, we present the start-to-end simulations for an XFELO based on both 4 GeV LCLS-II beam and 8 GeV LCLS-II-HE beam.

---

* qinweilun@pku.edu.cn, also at SLAC.

LAYOUT

The layout of the proposed linac-XFELO is sketched in Fig. 1. A photoinjector is used to generate high-brightness electron beams, and the 1.3 GHz superconducting linac cavities accelerate the beam to 4 GeV for LCLS-II and 8 GeV for LCLS-II-HE. Since the XFELO usually operates at lower current compared with high gain FELs, two stages of bunch compression are used to compress the beam to 100 A level current. A 3.9 GHz harmonic cavity is located before the first compressor to linearize the longitudinal phase space. The accelerated beam is transported for 2 km to the Beam Switch Yard (BSY) and directed to End Station A (ESA), a possible location for the XFELO. Since there is a beam energy chirp after the transport, a passive, parallel-plate corrugated dechirper [14, 15] is employed to cancel the energy chirp before entering the XFELO. The X-ray cavity is in the four crystal configuration as proposed in Ref. [6]. Diamonds are used as high reflectivity mirror for X-rays. For harmonic setup, phase shifters are used to suppress the fundamental wavelength [7].
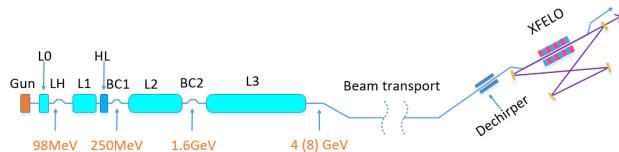
Figure 1: Layout of the proposed XFELO at the LCLS-II.

INJECTOR SIMULATION

Baseline of the LCLS-II injector [16] is based on the Advanced Photoinjector Experiment (APEX) [17] design, consisting of a normal conducting rf (NCRF) gun at 186 MHz with up to 20 MV/m gradient, one 1.3 GHz 2-cell buncher, two emittance compensation solenoids and one standard cryomodule with 8 9-cell superconducting cavities. Laser pulses of 40 ps flat-top are irradiated to a semiconductor cathode to generate 100 pC electrons bunches. The beam energy exiting the gun is 750 keV and reaches about 100 MeV at the exit of the injector. Genetic optimization based on NSGA-II algorithm was applied in the design of the injector to minimize the beam emittance [18]. Figure 2 shows the ASTRA [19] simulated electron longitudinal phase space, current, slice energy spread and slice emittance of the 100 pC baseline case at the exit of the injector. The beam emittance is about 0.3 μm. The electron beam exhibits a Gaussian-like current profile.

To get flat final longitudinal phase space, one approach is to shape the beam current by shaping drive laser pulse
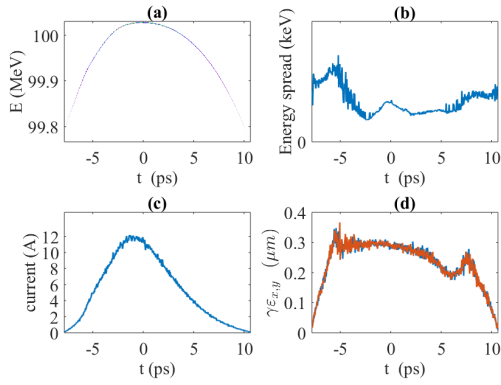
Figure 2: Electron longitudinal phase space, beam current, slice energy spread and slice emittance at injector exit for NCRF gun setup.
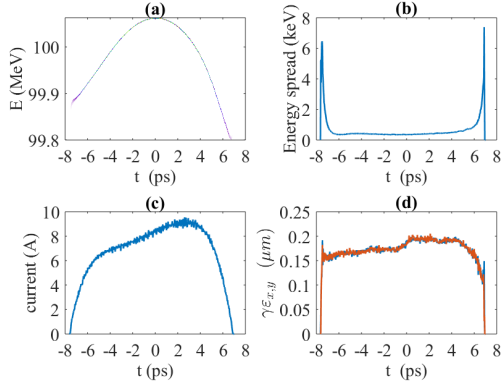
Figure 3: Electron longitudinal phase space, beam current, slice energy spread and slice emittance at injector exit for SCRF gun setup.

Figure 4: Electron longitudinal phase space, beam current, slice energy spread and slice emittance after linac optimization, using NCRF injector beam.
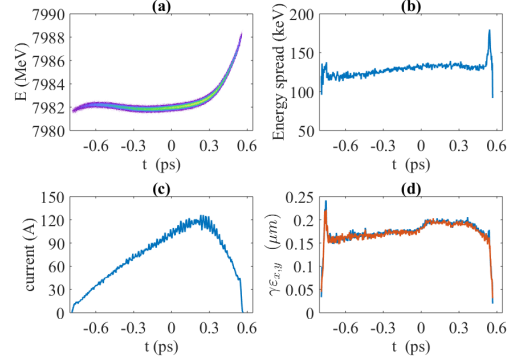
Figure 5: Electron longitudinal phase space, beam current, slice energy spread and slice emittance after linac optimization, using SCRF injector beam.

profile at the injector. Since the NCRF gun setup compresses the beam from 40 ps to 10 ps at relatively low beam energy of 750 keV, shaping the initial current strongly affects the envelope oscillation in the injector, leading to an increase in the projected beam emittance.

An alternative injector setup begins with one superconducing rf (SCRF) gun like the Wisconsin gun [20], which allows higher gun gradient up to 40 MV/m and the beam energy at the gun exit is near 4 MeV. The initial laser pulse is also reduced to 20 ps to reduce the bunch compression factor at low energy. The basic layout is kept the same as the NCRF setup except that the buncher is replaced with a 9-cell superconducting cavity, which requires a separate cryomodule. Figure 3 shows the final electron beam phase space distribution, current, slice energy spread and slice emittance for the case of the SCRF gun setup. The projected emittance is about 0.25 μm. The current profile is shaped to a ramped form with relatively sharp edges compared with the NCRF results.

LINAC SIMULATION

Several factors in the linac beam dynamics contribute to the final longitudinal phase space distribution, such as curvatures from the RF fields, nonlinearity from bunch compression and bunch wakefields from the linac, long transport

as well as the dechirper structure. We employ genetic algorithm with LiTrack [21] to optimize the linac parameters, including the gradient and the phase of the three main linacs as well as the harmonic cavity, the R_{56} of both bunch compressors and the parameters of the dechirper. For simplicity, beam energy at L1 end, L2 end and L3 end are fixed. The optimization objectives are set as the length of the flat part in the longitudinal phase space, defined as the bunch length within a specific energy spread, and the average beam current within the flat part. The optimized solution is then simulated using ELEGANT [22] with 1 M macroparticles.

Figure 4 and 5 show the ELEGANT simulated final beam phase space distribution, current, slice energy spread and slice emittance before the undulator for NCRF injector beam and SCRF injector beam, respectively. For the NCRF gun setup beam, the flat part of the beam is 400 fs, almost doubled compared with Ref. [10]. For the SCRF gun setup beam, the overall beam chirp is reduced and the flat part extends over 600 fs. The slice energy spread for both setup are well within 200 keV and the low slice emittance is maintained during the acceleration and transport.

FEL SIMULATION

With the electron beam from ELEGANT, we conducted GINGER [23] simulation to evaluate the XFELO performance. The XFELO adopts the proposed geometry in

Table 1: XFELO simulation parameters and output pulse properties (the repetition rate is assumed to be 1 MHz).

Parameter	4.9 keV	10 keV	14.4 keV	14.4 keV	14.4 keV	20 keV	24.2 keV
Electron gun	SCRF	SCRF	NCRF	NCRF	SCRF	SCRF	SCRF
FEL K	3.2128	2.0125	1.4304	1.4837	1.4837	1.0125	1.1539
E_{beam} [GeV]	7.982	7.982	3.994	7.982	7.982	7.982	7.982
Q [pC]	15	50	100	100	100	100	100
ε_n [μm]	0.25	0.25	0.35	0.35	0.25	0.25	0.25
σ_E [keV]	130	130	70	70	130	130	130
λ_u [cm]	2	2	2.6	2	2	2	1.5
N_u	1000	1000	1250	1000	1000	1000	2000
harmonic number	1	1	5	1	1	1	1
Z_R [m]	10	10	10	10	10	10	15
Bragg crystal	C(220)	C(440)	C(733)	C(733)	C(733)	C(880)	C(888)
Output coupling	4%	4%	4%	4%	4%	4%	5%
Pulse energy [μJ]	3.1	21	0.3	7	28	11	4.4
Spectral FWHM [meV]	10.9	5.4	5.8	3.9	3.4	2.7	1.3
Temporal FWHM [fs]	138	530	400	557	693	905	1989
$\sigma_\tau \sigma_\omega$ (FWHM)	2.27	4.37	3.52	3.26	3.58	3.67	4.06
# of Photons/pulse	3.9×10^9	1.3×10^{10}	1.3×10^8	3.1×10^9	1.2×10^{10}	3.4×10^9	1.1×10^9
Spectral flux [ph/s/meV]	3.6×10^{14}	2.4×10^{15}	2.2×10^{13}	7.9×10^{14}	3.6×10^{15}	1.3×10^{15}	8.5×10^{14}

Ref. [6] with four high-reflectivity diamond crystals to allow tuning of the central photon energy. Two sets of compound refractive lenses (CRLs) are used to provide focusing for the XFELO cavity. One of the four crystal is made thinner to allow for 4% output of the X-ray power.
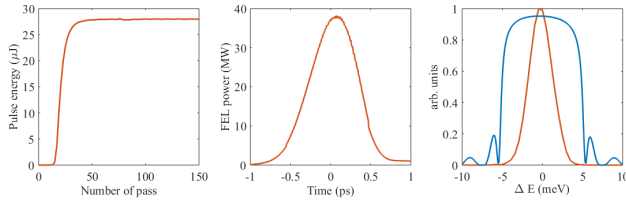
Figure 6: XFELO performance for 14.4 keV using 0.25 μm emittance, 130 keV slice energy spread and over 500 fs flat part beam with the SCRF gun setup.

XFELO parameters and performance are summarized in Table 1. For the 4.9 keV and 10 keV case, only part of the whole bunch is simulated to avoid spiky output of the spectra since the spectral acceptance is relatively large and the useful part of beam is long enough. For the NCRF gun setup, XFELO operating in 5th harmonic mode at 14.4 keV can generate X-rays with about 1.3×10^8 photons/pulse. XFELO operating in fundamental mode can generate much higher pulse energy than 5th harmonic mode thanks to higher single pass gain, reaching 3×10^9 photons/pulse. With higher gain, longer part of the beam contributes to lasing and the bandwidth is decreased. With the SCRF gun setup, the smaller emittance and the longer flat part of the beam result in a factor of four increase of output pulse energy. High flux X-rays with 1.2×10^{10} photons/pulse at 14.4 keV can be reached, corresponding to 3.6×10^{15} photons/s/meV spectral flux assuming 1 MHz repetition rate. The corresponding

pulse energy evolution, temporal profile as well as spectrum for this case are shown in Fig. 6. It should be noted that if the emittance of the SCRF gun setup is the same as the NCRF gun setup (0.35 μm), the output photons drop to about 6.5×10^9 photons/pulse, still a factor of 2 better than the NCRF gun setup. XFELO performance at higher photon energy up to 24.2 keV can also generate 10^9 photons/pulse with narrower bandwidth.

CONCLUSION

We performed the start-to-end simulations for XFELO driven by high repetition rate electron beams at the LCLS-II and the LCLS-II-HE. Two injector setup, one based on normal conducting APEX design and one based on superconducting gun design of the Wisconsin gun, are optimized using a genetic optimizer to obtain low emittance for the XFELO. The drive laser distribution of the SCRF setup is also shaped to obtain current ramp for phase space linearization. The parameters of the acceleration and beam manipulation components, i.e., the linac, bunch compressor and the dechirper, are optimized with a genetic algorithm based LiTrack optimizer to obtain flat phase space distribution over the length of 500 fs. The XFELO performance with various beam parameters in a photon energy range of 5-25 keV are evaluated with the start-to-end simulation. In the case of 8 GeV beam with the APEX type injector, about 10^9 photons per pulse with meV level bandwidth can be generated. With low emittance SCRF gun setup and drive laser shaping, the output at 14.4 keV is 1.2×10^{10} photons/pulse with 3.4 meV spectral bandwidth, corresponding to 3.6×10^{15} photons/s/meV spectral flux. The high flux and wide photon energy coverage makes the XFELO an unique source com-

plementary to the high gain XFELs for exciting scientific applications.

ACKNOWLEDGEMENT

REFERENCES

[1] P. Emma, et al., "First lasing and operation of an ångstrom-wavelength free-electron laser", Nature Photonics 4, 641 (2009).

[2] A. Kondratenko, et al., Part. Accel. 10, 207 (1980).

[3] R. Bonifacio, et al., "Collective instabilities and high-gain regime in a free electron laser", *Opt. Commun.* 50, 373 (1984).

[4] J. Amann, *et al.*, "Demonstration of self-seeding in a hard-X-ray free-electron laser", *Nature Photonics* 6, 693 (2012).

[5] K.-J. Kim, et al., "A proposal for an X-ray free-electron laser oscillator with an energy-recovery linac", *Phys. Rev. Lett.* 100, 244802 (2008).

[6] K.-J. Kim, et al., "Tunable optical cavity for an x-ray free-electron-laser oscillator", *Phys. Rev. ST Accel. Beams* 12, 030703 (2009).

[7] J. Dai, et al., "Proposal for an X-ray free electron laser oscillator with intermediate energy electron beam", *Phys. Rev. Lett.* 108, 034802 (2012).

[8] R. R. Lindberg, et al., "Performance of the x-ray free-electron laser oscillator with crystal cavity", Phys. Rev. ST Accel. Beams 14, 010701 (2011).

[9] SLAC National Accelerator Laboratory, *Linac Coherent Light Source II Conceptual Design Report*, No. SLAC-R-978 (2011).

[10] T. J. Maxwell, et al., "Feasibility study for an X-ray FEL oscillator at the LCLS-II", IPAC'15, Richmond, VA, USA, TUPMA028.

[11] J. Zemella, et al., "Time dependent study for an xray FEL oscillator at LCLS-II", FEL'15, Daejeon, Korea, TUP030.

[12] LCLS-II-HE "First Experiments" Meeting: Chemistry and Materials Physics, https://portal.slac.stanford.edu/sites/conf_public/lclsiihe2017/Pages/default.aspx.

[13] W. Qin, et al., "Beam Optimization Study for an X-ray FEL Oscillator at the LCLS-II", IPAC'16, Busan, Korea, WEPOY019.

[14] K. Bane, G. Stupakov, "Corrugated pipe as a beam dechirper", Nucl. Instru. and Methods A, 2012. 690: p. 106-110.

[15] Z. Zhang, et al., "Electron beam energy chirp control with a rectangular corrugated structure at the Linac Coherent Light Source" Phys. Rev. ST Accel. Beams 18, 010702 (2015).

[16] J. F. Schmerge, et. al., "The LCLS-II Injector Design", FEL'14, Basel, Switzerland, THP042.

[17] D. Filippetto, et. al., "APEX: A photo-injector for high average power light sources and beyond", FEL'14, Basel, Switzerland, TUA01.

[18] C. F. Papadopoulos, et al., "RF injector beam dynamics optimization for LCLS-II" IPAC'14, Dresden, Germany, WEPRO015.

[19] K. Flottmann, "ASTRA: A Space Charge Tracking Algorithm", user's manual available at http://www.desy.de/~mpyflo/Astra_dokumentation.

[20] J. Bisognano, et. al., NAPAC'13, Pasadena, USA, p622.

[21] K.L.F. Bane, et al., PAC'05, Knoxville, Tennessee, FPAT091 (2005).

[22] M. Borland, "Elegant: A flexible SDDS-Compliant Code for Accelerator Simulation", Advanced Photon Source Report No. LS-287, (2000).

[23] W. M. Fawley, "A User Manual for GINGER-H and its Post-Processor XPLOTGINH", Version 2.0k, June 2012.